Environmental Technology & Innovation 40 (2025) 104390

Contents lists available at ScienceDirect

Environmental Technology & Innovation

journal homepage: www.elsevier.com/locate/eti

Efficient aqueous degradation of fluoranthene using non-thermal plasma treatment

Djakaou Iya-Sou [a,b,*], Chedly Tizaoui [c,**], Nofel Merbahi [a,**], Jalloul Bouajila [d]

[a] Laboratoire Plasma et Conversion d'Energie (LAPLACE), Université Toulouse, INP, UMR CNRS 5213, Toulouse 31062, France
[b] Department of Chemical Engineering, School of Chemical Engineering and Mineral Industries, University of Ngaoundéré/Cameroon, BP 454, Ngaoundéré, Cameroon
[c] Water and Resources Recovery Research Lab, Department of Chemical Engineering, Faculty of Science and Engineering, Swansea University, Swansea SA1 8EN, United Kingdom
[d] Laboratoire de Génie Chimique, Université de Toulouse, CNRS, INP, UT, Toulouse F-31062, France

ARTICLE INFO

Keywords:
Non-thermal plasma
Advanced oxidation processes
Fluoranthene
Hydroxyl radicals
Fukui function

ABSTRACT

Fluoranthene (FLT), a polycyclic aromatic hydrocarbon (PAH) classified as a Priority Hazardous Substance, is recognised for its persistence in the environment. This is due to its complex molecular structure and low aqueous solubility, making it particularly challenging to degrade. This study investigated a pin-to-water non-thermal plasma (NTP) reactor for the efficient degradation of FLT in aqueous environments. The Results showed that NTP eliminated FLT rapidly with 100 % degradation in less than 5 min. A linear correlation was observed between the pseudo-first-order reaction rate constant and the applied voltage, with energy efficiency reaching up to 110 mg/kWh. The stable species and physicochemical parameters measured in the liquid phase show varying changes over time, both in the presence and absence of FLT. For instance, the pH of the solution decreased from around 6.6 to 4.5 while the oxidation-reduction potential (ORP) increased steadily as the discharge time increased. H_2O_2 concentrations revealed its consumption during the first 10 min of plasma exposure, indicating H_2O_2 contribution to FLT degradation. Additionally, LC-ESI-MS/MS analysis identified nine by-products, primarily resulting from nitration and hydroxylation reactions. Both LC-ESI-MS/MS analysis and Fukui function indices determined through Density Functional Theory calculation provided insights into the reaction mechanism. Overall, this study highlights the effectiveness and potential of NTP for the treatment of PAH-contaminated waters.

1. Introduction

Fluoranthene (FLT) is a harmful substance to both humans and the environment. It has been listed as a substance of very high concern (SVHC) under the EC REACH Regulation (EC/1907/2006) and a priority hazardous substance and ubiquitous persistent, bio accumulative and toxic (uPBT) compound under the Water Framework Directive (2008/105/EC amended by 2013/39/EU). The US Environmental Protection Agency (US EPA) has also classified FLT as a priority pollutant (Environmental Protection Agency). FLT

* Corresponding author at: Laboratoire Plasma et Conversion d'Energie (LAPLACE), Université Toulouse, INP, UMR CNRS 5213, Toulouse 31062, France.
** Corresponding authors.
E-mail addresses: iya-sou@laplace.univ-tlse.fr (D. Iya-Sou), c.tizaoui@swansea.ac.uk (C. Tizaoui), merbahi@laplace.univ-tlse.fr (N. Merbahi).

https://doi.org/10.1016/j.eti.2025.104390
Received 22 April 2025; Received in revised form 5 July 2025; Accepted 19 July 2025
Available online 20 July 2025

(C_6H_{10}) is a representative polycyclic aromatic hydrocarbon (PAH) with a fused structure consisting of naphthalene and benzene rings connected via a five-membered unit. Due to its rigid molecular structure, FLT is highly persistent in the environment, accumulating in biota and throughout the food chain (Styszko et al., 2025). It has been detected in various environmental media including surface water (Wu et al., 2023; Tovar-Salvador et al., 2025), groundwater (Montgomery, 2007), and wastewater (Tovar-Salvador et al., 2025). It has also been detected even in human milk (Galindo et al., 2025). Exposure to FLT has been linked to kidney and liver diseases, as well as cancers (Agency for Toxic Substances and Disease Registry (US), 1995; Boström et al., 2002; Zhang et al., 2024). A systematic review highlighted that human exposure to PAH-contaminated water sources significantly increases cancer risk among both children and adults, with ingestion and dermal absorption being primary exposure pathways (Ziyaei et al., 2024). Additionally, FLT can disrupt enzymatic activity and damage cellular structures, impairing the antioxidant capacity of organisms (Sun et al., 2020). Thus, its persistence in water bodies further exacerbates its ecological impact, leading to chronic effects on aquatic species' reproduction and growth, disrupting ecosystems and food chains.

Although FLT is not intentionally manufactured, it naturally occurs in fossil fuels such as coal, oil, and bitumen. Consequently, FLT enters aquatic environments through various pathways, including point source releases (e.g. wastewater discharges or fuel leaks), diffuse sources (e.g. road transport), and atmospheric deposition following rainfall events. A 2024 study revealed that fluoranthene was detected in 80 % of water catchments across England, often at concentrations exceeding statutory limits (Annual Average Environmental Quality Standard (AA-EQS): 0.0063 μg/L; Maximum Allowable Concentration (MAC-EQS): 0.12 μg/L), especially in runoff from roads like the motorway M6 in England (Hosea and Salvidge, 2024; EA&DEFRA, 2025). Historical industrial contamination, particularly in soils and sediments, has also been identified as a significant source of PAHs, including FLT, in water systems (Zhang et al., 2019). According to pollution inventory data from the UK Environment Agency, urban wastewater treatment facilities are the largest point source of PAH releases to water, followed by refineries, and iron and steel works (Environment Agency, 2019). This highlights the significant contribution of these industries to environmental contamination, particularly in relation to polycyclic aromatic hydrocarbons (PAHs).

Given the environmental and health risks posed by FLT and its widespread occurrence and persistence in aquatic environments, effective monitoring and remediation strategies for FLT are, therefore, essential. Its detection in the majority of water catchments stresses its significance as an environmental pollutant. In this context, advanced oxidation processes (AOPs), which utilise highly reactive oxidative species such as hydroxyl radicals ($^{\bullet}OH$), have gained attention for their potential in wastewater treatment (Tufail et al., 2020; Ji et al., 2024). Among AOPs, non-thermal plasma (NTP) distinguishes itself with its flexibility, efficiency, chemical-free operation, and capacity to target a broader spectrum of contaminants. NTP generates a variety of reactive oxygen and nitrogen species (RONS) that work synergistically to degrade not only pharmaceuticals, dyes, pesticides, and pathogens but also complex PAH molecules (Abdelaziz et al., 2018; Machala et al., 2019; Abbas et al., 2020; Bilea et al., 2024; Iya-Sou et al., 2024, 2025; Wang et al., 2025). To be effective, the RONS generated in the plasma must be transferred to the water through the gas/water interface. This transfer is critical, as the concentration of RONS in the liquid phase depends on several factors, including the type of plasma reactor, working gas, power source, treatment duration, and the volume of treated liquid. Additionally, the production of RONS can lead to pH changes in the water, which further enhances the oxidation of pollutants. This combination of chemical and physical processes is a key strength of NTP, allowing it to address persistent pollutants like PAHs, whose complex chemical structures make them particularly challenging to degrade. Furthermore, since NTP does not require the addition of chemicals to generate RONS, it is considered an environmentally friendly technology, especially when powered by renewable energy sources.

Several NTP reactors have been studied for wastewater treatment to degrade organic contaminants such as dyes, phenols, and pharmaceuticals, with the most common being corona discharge (Bilea et al., 2024), dielectric barrier discharge (Gao et al., 2013; Khourshidi et al., 2024), plasma jet (Hamdan et al., 2018), and gliding arc discharge (Djakaou et al., 2015; Kong et al., 2019). However, studies on the degradation of PAHs in water using NTP remains scarce, making direct comparisons with existing studies difficult. Thus, our work uniquely targets FLT. By doing so, we expand the scope of NTP research and provide compelling evidence for its broader applicability in the remediation of hazardous environmental pollutants, where other technologies, such as incineration or bioremediation are limited. Our study employs an NTP reactor configured as an array of high-voltage pins positioned above the water surface to maximise interaction of the discharge with FLT, which tends to accumulate at the air-water interface, being a hydrophobic compound. This configuration enhances the efficiency of plasma-induced degradation by targeting FLT where it is most concentrated.

The goal of this study was to deepen understanding of FLT degradation via NTP and examine how this AOP influences the kinetics and degradation products of this priority hazardous pollutant. Experiments were conducted using plasma generated above the water surface at atmospheric pressure in open air, with varying discharge gaps, pulse durations, frequencies, and voltages. Additionally, the dynamic changes in FLT degradation by-products were identified through liquid chromatography coupled with electrospray ionisation triple-quad mass spectrometry (LC-ESI-MS/MS), alongside a Fukui function index approach to predict the underlying degradation mechanisms. This study provides valuable insights into the degradation of FLT by NTP and demonstrates the high reactivity and efficiency of this chemical-free AOP, positioning it as a powerful tool in environmental remediation and waste management.

2. Experimental section

2.1. Chemicals

All chemicals used in this study were of reagent grade, and solvents were of HPLC grade. Fluoranthene (purity≥98 %) and hydrogen peroxide (30 %V) were sourced from Sigma-Aldrich, and HPLC-grade methanol and acetonitrile were obtained from Fisher Scientific. Deionised water (DW) was used throughout the study to eliminate potential interference from ions commonly present in tap water,

ensuring a more accurate understanding of plasma discharge effects and the potential degradation mechanisms of the target pollutant. Aqueous FLT solutions were prepared from a stock solution of FLT dissolved in methanol at a concentration of 1 g/L. The appropriate volume of the methanol solution was transferred to the reactor and allowed to completely evaporate before adding the required volume of deionised water and thoroughly mixing the solution. Due to its low solubility in water, which is reported to range from 200 to 265 μg/L (EPA, 1980; PubChem, 2023), FLT was prepared in aqueous solutions at concentrations not higher than 0.2 mg/L.

2.2. Experimental procedure

The NTP reactor featured an array of seven tungsten multi-pin high-voltage (HV) electrodes mounted on three copper bars positioned across the surface of the circular reactor (Fig. 1). Each electrode has a diameter of 1 mm, a length of 100 mm, and a curvature radius of 100 μm. The electrodes were evenly spaced with a fixed inter-tip distance of 28 mm across the copper bar and connected to a pulsed power supply via the copper bars, representing the high voltage electrodes. The pins were cleaned prior to experiments, and their curvature radius and condition are examined using an optical microscope. Pins showing significant etching were not reused. The ground electrode (cathode) was a copper ribbon (2 cm width), which surrounded the outside diameter of the reactor. The ribbon was sufficiently wide to cover the entire height of the liquid to be treated. The reactor was a cylindrical Pyrex® glass dish of 90 mm (OD) and 88 mm (ID). The overall dish height was 55 mm, while the liquid height was approximately 17 mm. A micro-control system, holding the HV electrodes, allowed precise adjustment of the gap distance between the electrode tip and the liquid surface. The streamers generated by the seven HV electrode tips covered the majority of the liquid surface. The placement of the cathode was made in a way to align the electric fields toward the plasma-treated liquid, enhancing the transport and diffusion of plasma species from the gas phase to the liquid phase.

Ambient air at room temperature with a relative humidity (RH) of 52.5 ± 0.5 % was used as the working gas and the operating parameters examined in this study included electrode tip-to-water surface gap distances, pulse duration, voltage, and pulse frequency. The solution temperature was about 23 °C before treatment and its value did not change by more than 2 °C during treatment. The volume of the solution was 100 mL and FLT concentration was 0.2 mg/L. A magnetic stirrer was set to a speed of 150 rpm was used to ensure homogeneous mixing of the solution. This rotational speed of stirrer was carefully chosen so the formation of vortices in the liquid were avoided, and a consistent electrode tip-to-water surface gap was maintained.

The power supply device consisted of an appropriate push-pull solid-state circuit high voltage pulse PVX 4110 at the output of a DC

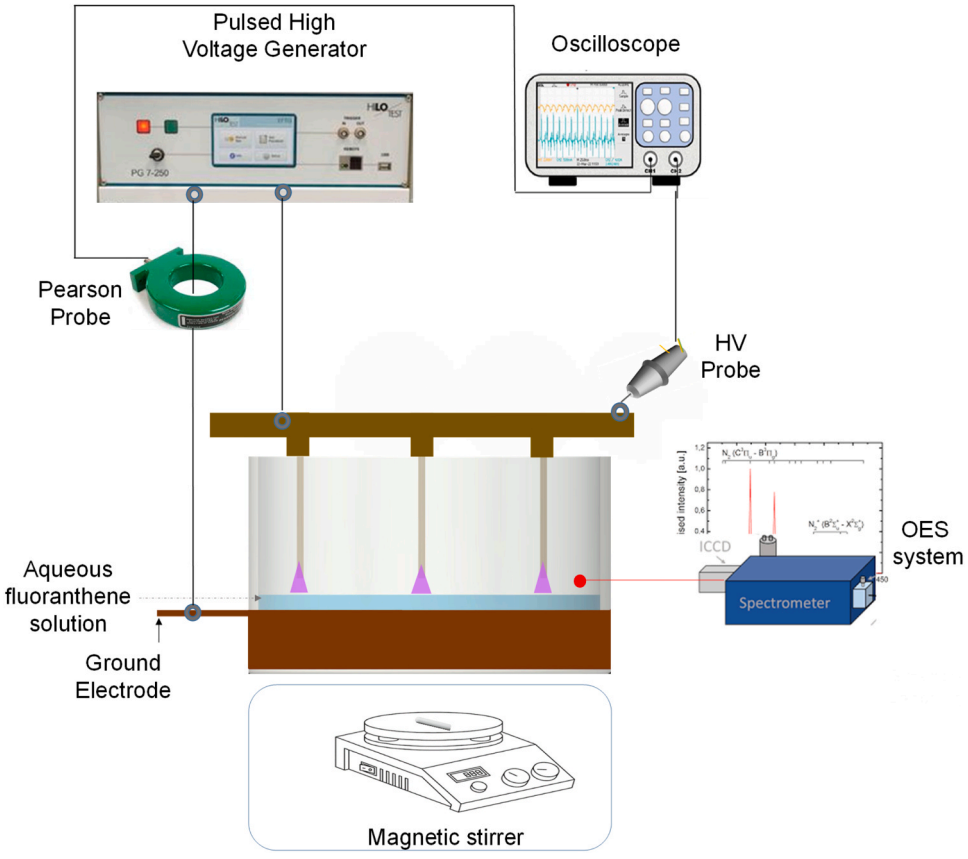

Fig. 1. Experimental set up of the non-thermal plasma reactor.

high-voltage generator (Technix HV SR10-R-300). This system provides pulses of voltages from 0 to 10 kV, frequencies up to 10 kHz, and pulse widths in the range 500 ns to 100 ms. Probes were used to monitor the applied voltage (Tektronix P6015A with a maximum voltage rating of 40 kV pk PULSE) and current (Pearson current monitor model 4100, maximum peak current 500 A, high frequency 35 MHz), linked to a digital oscilloscope (WaveSurfer 10, 1 GHz and 10GS/s). The discharge current was obtained by subtracting the displacement current (capacitive current), previously measured without discharge.

The characterisation of the short-lived primary species in the gas phase near the gas/liquid interface was performed using an Acton SP 2750 optical emission spectrometer (Teledyne Princeton Instruments, USA) with a focal wavelength of 0.75 m. The latter is equipped by three diffraction gratings of values 2400, 1800, and 600 tr/mm blazed respectively at 250, 500, and 500 nm. In this work, only the first two gratings were used to obtain an emission spectrum from 200 to 800 nm. The photons emitted by the discharge were collected using a 600 μm diameter optical fibre connected to the spectrometer. To prevent the second-order UV spectra from being superimposed on the visible spectra, a UV blocking filter was placed in front of the fibre. Data acquisition and processing were performed using WinSpec32 processing software.

2.3. Analytical methods

The detection and quantification of nitrates (NO_3^-), nitrites (NO_2^-) and hydrogen peroxide (H_2O_2) in plasma-treated water, both with and without fluoranthene (FLT), were conducted via multiphotometric analysis. A digital absorption spectrophotometer (UVline 9000 C, Aqualabo), equipped with specific reagents for target analyses, was used. The instrument was fitted with light-emitting diodes (LEDs), with measurement wavelengths set to 553, 530, and 533 nm, respectively, and a silicone detector. Electrical conductivity and pH measurements were made using a SevenGo Duo SG 25 multiparameter probe (Mettler Toledo).

The concentration of FLT was quantified using an HPLC system (Agilent 1260 Series, Germany), which was equipped with a binary pump and a fluorescence detector. Prior to analysis, excitation and emission wavelengths appropriate for FLT were optimised at 285 and 466 nm, respectively. FLT was analysed on a Supelco Ascentis Express C18 column with an isocratic mobile phase composed of 85 % acetonitrile and 15 % water, at a flow rate of 0.4 mL/min. The sample injection volume was 5 μL, and FLT's retention time was approximately 2.2 min. Data acquisition and analysis were performed using Agilent MassHunter software. Each dataset in the present study was replicated in at least three independent experiments. The reported data represent the means ± standard deviation.

The degradation efficiency of FLT and energy yield (mg/kWh) were calculated using Eqs. (1) and (2), respectively. Assuming pseudo-first-order reaction kinetics, the apparent FLT degradation kinetic constant (k) was evaluated using Eq. (3).

$$D \quad (\%) = \left(1 - \frac{C_t}{C_0}\right) \times 100 \tag{1}$$

$$Y = \quad \frac{C_0 \times V \times \frac{D}{100}}{P \times t} \tag{2}$$

$$-\ln\left(\frac{C}{C_0}\right) = k \times \mathrm{t} \tag{3}$$

where: D is the degradation efficiency (%), C_0 and C_t are FLT concentrations (mg/L) at treatment times 0 and t, respectively, Y is energy yield (mg/kWh), V is solution volume (L), P is the average power dissipated in the discharge (kW), t is plasma treatment time (h in Eq. (2) and min in Eq. (3)), and k is the apparent degradation kinetic constant (min^{-1}).

2.4. Identification of reaction products and mechanism

A triple quadrupole mass spectrometer (Ultivo QQQ, Agilent, Germany) was employed to analyse the reaction products formed during the treatment process over time. Samples were introduced using direct-injection electrospray ionisation (ESI) in negative mode, with a fragmentor voltage set to 135 V. Nitrogen served as the sheath gas, flowing at 11 L/min with a temperature of 250°C. Mass spectra were acquired within the m/z range of 50–500. Samples collected at different reaction times were analysed to track the change of the products' abundance versus time. Data were processed using Mass Hunter Quantitative Analysis 10.2 to calculate peak areas for each significant m/z [M-H] across the various samples. The chemical structures of the degradation products were further confirmed through collision-induced dissociation (CID) with nitrogen as the collision gas.

To provide insights into the reaction mechanism, mass spectrometry data were complemented by computational chemistry calculations performed with Gaussian 16 W and Multiwfn packages. Gaussian View 6.1 was used as interface. Molecular geometries were optimised using hybrid Density Functional Theory (DFT) with the B3LYP functional and the 6–31 G basis set. Electron density and electron orbits including HOMO and LUMO were also obtained utilising Gaussian software. Active sites were identified based on Fukui functions, which were calculated from Mulliken atomic charges derived from Gaussian analysis (Fei, 2012; Lu and Chen, 2012, 2020). The susceptibility of FLT to radical attack was assessed using the radical Fukui function index (f^0) as defined by Eq. (4). A higher value of f^0 at a specific site indicates an increased reactivity of that site toward radical species (Farooq et al., 2023). The Fukui indices, f^- and f^+, also provide insight into sites vulnerable to electrophilic and nucleophilic attacks, respectively. The Fukui indices are calculated as follows:

$$f^0 = \frac{f^+ + f^-}{2} \tag{4}$$

$$f^+ = \rho(N = N_0 + 1) - \rho(N = N_0) \tag{5}$$

$$f^- = \rho(N = N_0) - \rho(N = N_0 - 1) \tag{6}$$

Where: f^0, f^+, and f represent the Fukui functions for radical, nucleophilic (where the total number of electrons in a molecule increases by one), and electrophilic (where the total number of electrons decreases by one) reactions, respectively. In these equations, $\rho(N = N_0)$, $\rho(N = N_0+1)$, and $\rho(N = N_0\text{-}1)$ denote the atomic charges in the molecule (Mulliken charges are used in this study) with electron counts of N_0, N_0+1, and N_0-1, respectively; N_0 is the total number of electrons in the original molecule before adding an electron (N_0+1) or removing an electron (N_0-1).

3. Experimental results and discussion

This section of the results first explores the effect of key operating parameters including the gap distance between the electrode tips and the water surface, pulse frequency, and pulse width on the elimination of FLT. Next, the influence of applied pulse voltage on FLT degradation and energy efficiency is examined. The results section also addresses the by-products generated during FLT degradation and proposes a mechanism for FLT breakdown in the NTP reactor.

3.1. Effect of electrode tip-to-water surface gap, pulse frequency, and pulse width on FLT degradation

The degradation of FLT was examined under various conditions, including electrode tip-to-water surface gap distances, pulse frequencies, and pulse widths, with results shown in Fig. 2. FLT removal occurred rapidly across all tested parameters, with more than 80 % degradation typically achieved within 5 min of exposure to the plasma.

The effect of the electrode tip-to-water surface gap on FLT degradation, for a fixed input voltage of 10 kV, frequency of 10 kHz, and pulse width of 1μs, shows that the gap distance and degradation efficiency exhibit an inverse relationship; when one increases, the other decreases. For example, at a reaction time of 10 min, the degradation efficiency, D, increased from 85 % to 100 % as the gap was reduced from 10 mm to 4 mm. This trend can be attributed to the inverse relationship between the gap distance and pulse power, as shown in Fig. 2a and Table S1. As the gap increases, the electric field strength decreases, since $E = V/d$, making the field less effective at ionising the gas. This results in fewer micro-discharges, which diminishes the overall plasma activity and reduces the generation of reactive species responsible for degradation. Furthermore, the DBD plasma system can be simulated as a capacitor, meaning that increasing the gap lowers the capacitance, thereby reducing the charge stored and released per pulse. This ultimately leads to lower energy and power being dissipated in the system. These results can be attributed to more intense streamer branching when the ground electrode is closer to the high-voltage electrode (i.e. smaller gap). This configuration also modifies the gas/liquid surface discharge current and increases the shock wave velocity, both of which contribute to improved degradation efficiency (Locke et al., 2006; Dickenson et al., 2021; Furusato et al., 2022; Iya-Sou et al., 2025). Although the smallest gap of 4 mm resulted in the highest degradation efficiency, it was challenging to maintain a stable plasma under this condition. Therefore, a 6 mm gap, offering a balance between performance (96 % degradation at a reaction time of 10 min) and plasma stability, was selected for the remainder of the experiments.

The results observed for the effect of pulse width (at 10 kV, 10 kHz, 6 mm) and frequency (at 10 kV, 1 μs, 6 mm) on FLT elimination (Fig. 2b and c) are antagonistic: good efficiency is observed for high frequency values (10 kHz), in contrast to the effect of pulse width, where good efficiency was obtained for lower pulse width (0.5 and 1 μs). This variation in frequency correlates with the pulse power injected into the reactor, as detailed in Table S1. For a constant pulse width, the plasma reaction time, which is proportional to the frequency (the phase following discharge generation during the pulse duration), effectively prolongs the excitation, dissociation and

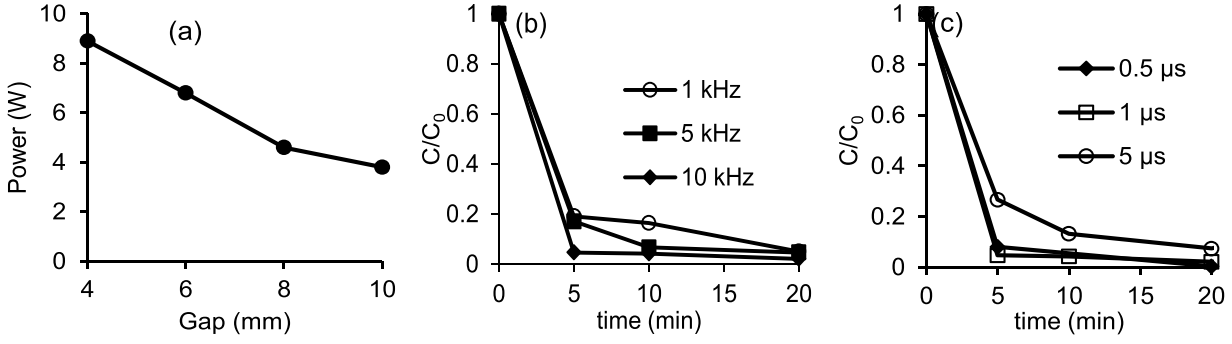

Fig. 2. Effect of power supply parameters on fluoranthene degradation (a) electrode tip-to-water surface gap (b) pulse frequency, and (c) pulse width (Error bars (<5 %) are too small to show on the graph; Voltage =10 kV, C_0 =0.2 mg/L; V =100 mL).

ionisation processes of the main air molecules to form highly reactive species such as primary radicals (•O, •N, •OH…), metastable species (N_2(A3Σ+u)) and ions (N^+, O^+, N_2^+, O-, etc.) and relatively stable molecules such as H_2O_2 (Shao et al., 2018). According to Table S1, as the frequency was raised from 1 to 10 kHz, the power increased by a factor of 15 while the degradation efficiency at a reaction time of 10 min increased from 84 % to 96 %, respectively. Other studies have also reported increased degradation efficiencies as the pulse frequency increased (Zhan et al., 2018; Bilea et al., 2024).

As shown in Table S1, pulse power varies with both the electrode tip-to-water surface distances, frequency and the applied voltage. This variation in input pulse power is consistent with the results observed in Fig. 2b and c. However, the effect of pulse width on FLT removal cannot be fully explained by pulse power alone. At a constant frequency, pulse width influences the electric field through the Joule effect which in turn affects the types of species generated by the discharge. Longer pulse widths allow current to flow for extended durations, resulting in greater thermal energy deposition in the plasma. This increases Joule heating, reduces energy efficiency for chemical reactions, and raises the risk of arc formation and uncontrolled discharges leading to additional energy losses. In contrast, short pulse widths deliver high peak power over brief periods, creating energetic electrons while keeping the overall gas temperature relatively low. This minimises Joule heating and energy loss to heat, thereby enhancing the generation of reactive species such as radicals, which drive the degradation process. Previous studies on plasma-liquid interactions have also demonstrated that at lower discharge temperatures, highly reactive oxygen species are favored while at higher temperatures, nitrogen species dominate due to the higher bond dissociation energy of N_2 compared to oxygen (Machala et al., 2019; Tachibana and Nakamura, 2019).

3.2. *Effect of applied voltage on FLT degradation and energy yield*

Fig. 3 illustrates the influence of applied voltage, ranging from 6 to 10 kV, on FLT degradation, the reaction rate constant for FLT elimination in solution, and on energy efficiency. Fig. 3a shows a significant improvement in FLT degradation efficiency as both applied voltage and plasma treatment time increase. For instance, after 5 min of plasma treatment, FLT degradation efficiency rises from 25 % to 95 % when the applied voltage increases from 6 to 10 kV. In comparison with other AOPs, only 80 % of FLT were removed after 2 h photocatalysis (Bai et al., 2017) while a better degradation efficiency than photocatalysis of 95 % was demonstrated using γ-rays irradiation at a dose rate of 60 Gy/min of FLT solution for 13 min (time was calculated from the data in the reference) (Popov and Getoff, 2005). Thus, electrical discharge plasma above the liquid surface is highly effective in degrading FLT as other water contaminants such as pharmaceuticals, pesticides, and pathogenic microorganisms, through the generation of highly oxidative species including hydroxyl radicals and nitrogen-based compounds (Murugesan et al., 2020). These reactive species diffuse from the gas-liquid interface into the water, initiating chemical reactions with the contaminants. Due to their limited penetration depth, the reactive species generated by NTP primarily act at the water surface. As FLT is a hydrophobic contaminant that tends to accumulate at the air-water interface, it becomes highly susceptible to radical-induced degradation, which could explain the high degradation efficiency observed in our study.

To clearly highlight the influence of voltage, Fig. 3b presents the relationship between the pseudo-first-order reaction rate constant (k) and the applied voltage. The rate constant increases linearly with voltage, with a proportionality coefficient of 0.133 $min^{-1}{\cdot}kV^{-1}$. This means that for every 1 kV increase, the rate constant increases by 0.133 min^{-1}, representing a substantial change. For example, when the voltage increases from 6 to 10 kV, the rate constant nearly increases sevenfold. Additionally, Fig. 3b indicates that voltages must exceed approximately 5.6 kV before any significant FLT degradation occurs, aligning with the observation that plasma ignition begins at around this threshold. It is also important to emphasise that, under the specific operating conditions employed in this study (applied voltage of 10 kV, a pulse repetition frequency of 10 kHz, a pulse width of 1 μs, and an electrode-to-water surface gap of 6 mm), the plasma discharge exhibited consistent stability throughout the entire treatment process. Notably, the discharge consistently operated within the streamer regime, maintaining a stable current profile for each pulse. This stability was observed to be independent of the treatment duration, indicating that the discharge characteristics remained robust and unaffected over time under these conditions. Such reproducibility is essential for ensuring the reliability of plasma treatments in practical applications.

Higher applied voltages result in greater energy input and an accelerated ion wind, which enhances turbulence in the water and

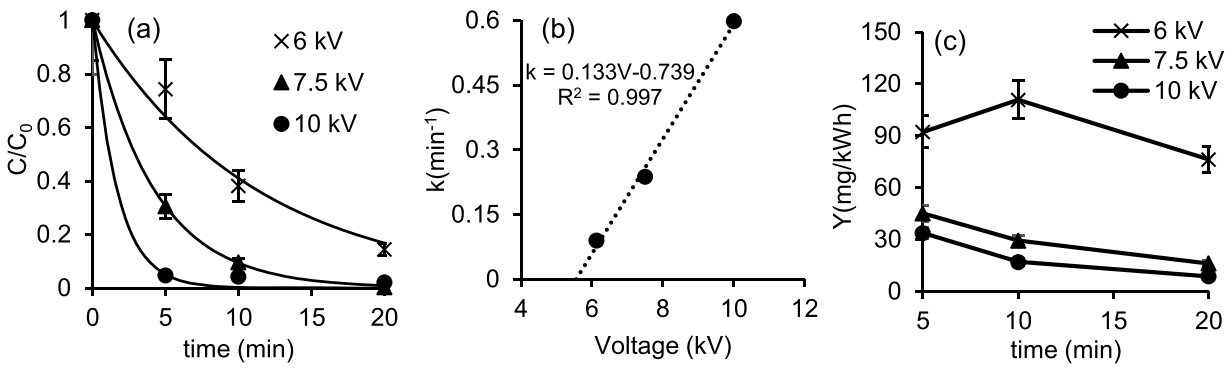

Fig. 3. Effect of applied voltage on (a) FLT degradation, (b) reaction rate constant, k, and (c) energy yield, Y (frequency = 10 kHz, gap = 6 mm, pulse width = 1 μs, C_0 = 0.2 mg/L; V = 100 mL).

improves mass transfer of reactive species in the liquid phase. With higher energy inputs, more reactive species (such as $^{\bullet}OH$, O_3, $ONOO^-$) are generated, facilitating the oxidation of FLT molecules in the liquid phase. This is due to an increased production of energetic electrons and enhanced excitation, ionisation, and dissociation reactions during plasma discharge (Bruggeman et al., 2016).

Fig. 3c presents the energy efficiency, showing that yield (Y), defined as the ratio of FLT mass eliminated per unit of energy consumed, increases as the applied voltage decreases. The figure also reveals that yield generally decreases as reaction time increases, suggesting that the plasma not only degrades the parent FLT molecule but also partially decomposes the by-products generated from FLT breakdown. Similar trends have been observed in other plasma-based organic molecule degradation studies (Gao et al., 2013; Wu et al., 2019). Yields ranged from an average of 93 mg/kWh (maximum 110 mg/kWh) at 6 kV to 20 mg/kWh at 10 kV were calculated in this study, indicating FLT's strong susceptibility to plasma degradation. In contrast, a study by Gao et al. (2013) reported significantly lower energy yields, ranging from 0.1 to 1 mg/kWh, for the degradation of other organic compounds in water using plasma systems. This discrepancy may be attributed to the presence of a dielectric barrier around the high-voltage electrode they used, which can limit discharge efficiency. The enhanced energy efficiency observed in our study is likely due to a more effective electrode configuration and the nature of FLT itself. As a hydrophobic compound, FLT tends to accumulate near the gas-liquid interface, resulting in increased exposure to reactive plasma species. Supporting this, Saleem et al. (2022) reported substantially higher energy yields, on the order of thousands of mg/kWh, for the degradation of hydrophobic per- and polyfluoroalkyl substances (PFAS), achieved by ensuring a dense spread of discharges across the entire liquid surface in their radial plasma reactor. These findings highlight the potential of NTP as a promising technology for the abatement of PAHs, an area where research remains relatively limited. However, to ensure practical applicability, careful evaluation is needed regarding its integration into real-world wastewater treatment plants. In actual wastewater streams, suspended solids (TSS) are commonly present, and pollutants such as FLT may adsorb onto these particles. The pin-to-water surface reactor configuration used in this study demonstrates notable potential for treating both dissolved contaminants and those associated with suspended matter. Reactive plasma-generated species interact with these particles, promoting the oxidation and degradation of surface-bound compounds such as FLT. In addition to contaminant breakdown, the process may also induce particle aggregation, facilitating the removal of TSS through improved solid-liquid separation. Evidence from the literature further suggests that NTP can support TSS dissolution, pointing to its potential for effective particulate destruction (Kim et al., 2020). Moreover, NTP could serve as a pre-treatment step, transforming biologically recalcitrant or inhibitory compounds into more biodegradable compounds. This would enhance subsequent biological treatment performance, enabling efficient contaminant removal while reducing overall treatment costs and carbon footprint (Nippatlapalli and Locke, 2022). Alternatively, NTP could be used as a post-treatment or polishing step after biological treatment, especially when effluent is discharged into sensitive environments. For instance, Xiong et al. (2019) demonstrated that coupling NTP with biodegradation for treating 1,4-dioxane resulted in degradation rates 3–5 orders of magnitude higher than previous studies, significantly lowering energy consumption and treatment time. Their work showed 25 % mineralisation via NTP, with the remaining 75 % transformed into intermediates that were readily biodegraded, illustrating the synergistic benefits of integrated treatment.

The decision to deploy NTP as a pre- or post-treatment step should be based on treatment objectives and wastewater characteristics,

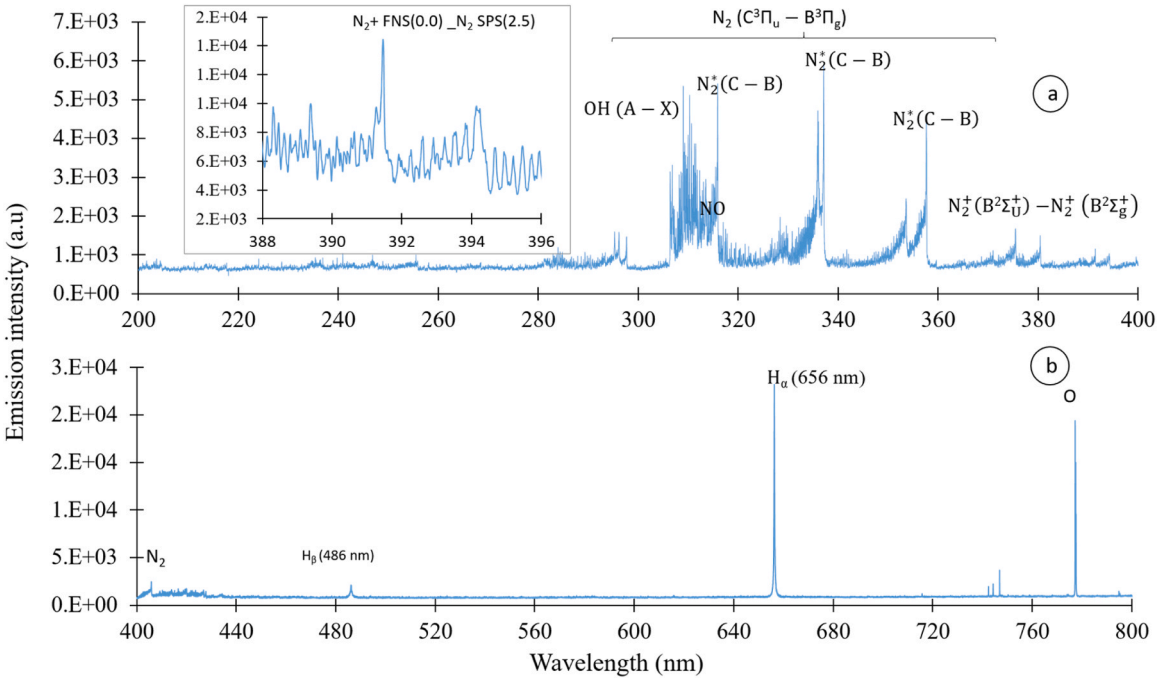

Fig. 4. UV and visible emission spectra (200–800 nm) of pulsed discharge above deionised water surface.

whether industrial or domestic. It is also important to consider that high TSS levels may hinder plasma generation and reduce the formation of reactive species, thus affecting treatment performance. For industrial applications targeting low concentrations of persistent pollutants (such as 0.2 mg/L FLT), optimising parameters such as electrode configuration, mixing, and power input becomes critical to ensure high energy efficiency. As no single treatment process is likely to be sufficient for eliminating recalcitrant contaminants, integrating NTP with existing biological or physical treatment technologies appears to be the most viable strategy. Such hybrid systems offer the potential for complete pollutant removal and improved cost-effectiveness, particularly when treating complex wastewater matrices. Ultimately, the integration of NTP, whether as a pre-treatment, post-treatment, or both, should be guided by careful assessment of treatment performance, energy efficiency, and economic viability.

3.3. Reactive species

To aid in the discussion of the FLT degradation mechanism by NTP, an assessment was made of the key reactive species likely formed in air-based plasma. This included optical emission characterisation of the short-lived primary species in the gas phase near the gas/liquid interface, as well as the analysis of stable species and physico-chemical parameters in the liquid phase, both in the presence and absence of the pollutant (FLT).

The UV and visible emission spectra (200–800 nm) obtained are displayed in Fig. 4. As illustrated in the figure, there is a predominance of nitrogen and oxygen species, characteristic of a discharge in humid ambient air, as is the case in our experiments. The characteristic bands of Second Positive System (SPS) N_2 ($C^3\Pi_u$-$B^3\Pi_g$) between 323 and 415 nm with a central peak at 337.1 nm is linked to the dissociation by electron impact of the N_2 molecule. We also observe the characteristic NO band between 250 and 300 nm, which is the result of the reaction between $N_2(C^3\Pi_u - B^3\Pi_g)$ and oxygen. The peaks obtained at 316, 337 and 357 nm are attributed to $N_2^*(C^3\Pi_u - B^3\Pi_g)$ which is well known for its reactivity in the nitration of compounds (Locke et al., 2025). Furthermore, the UV spectra demonstrate a band at 309 nm, attributed to the OH(A-X) emission spectrum, emitted by the discharge of corona sparks pulsed in air within the 306 and 310 nm range, and revealing the presence of the First Negative System of N_2^+ (391 nm). In the visible range (400–800 nm), N_2 bands were observed at 415 nm, H_β bands at 486 nm and a Gauss band at 656 nm (Hα). Additionally, the oxygen triplet line at 777 nm was also detected (Kooshki et al., 2024; Iya-Sou et al., 2025).

In summary, the electrons excite, dissociate and ionise air molecules, generating high concentrations of primary species (e.g. $^{\bullet}OH$, O, N, etc.) along each discharge filament from the high-voltage electrode tip to the water. These primary species then interact with surrounding air to form, through a series of chemical reactions, more stable secondary species (e.g. O_3, H_2O_2, $ONOO^-$, NO_3, NO_2, etc.) (Bruggeman et al., 2016; Shen et al., 2019). The reactive oxygen and nitrogen species (RONS) of interest are subsequently generated in the liquid phase (Bruggeman et al., 2016) via interactions between the primary and secondary species at the liquid surface leading to dissolved species in solution such as hydrogen peroxide, ozone, and nitrates.

The stable species and physico-chemical parameters measured in the liquid phase, both in the presence and absence of FLT, for plasma contact times up to 20 min under best conditions (10 kV, 6 mm gap, 10 kHz, 1 μs) are shown in Fig. 5. As illustrated, all

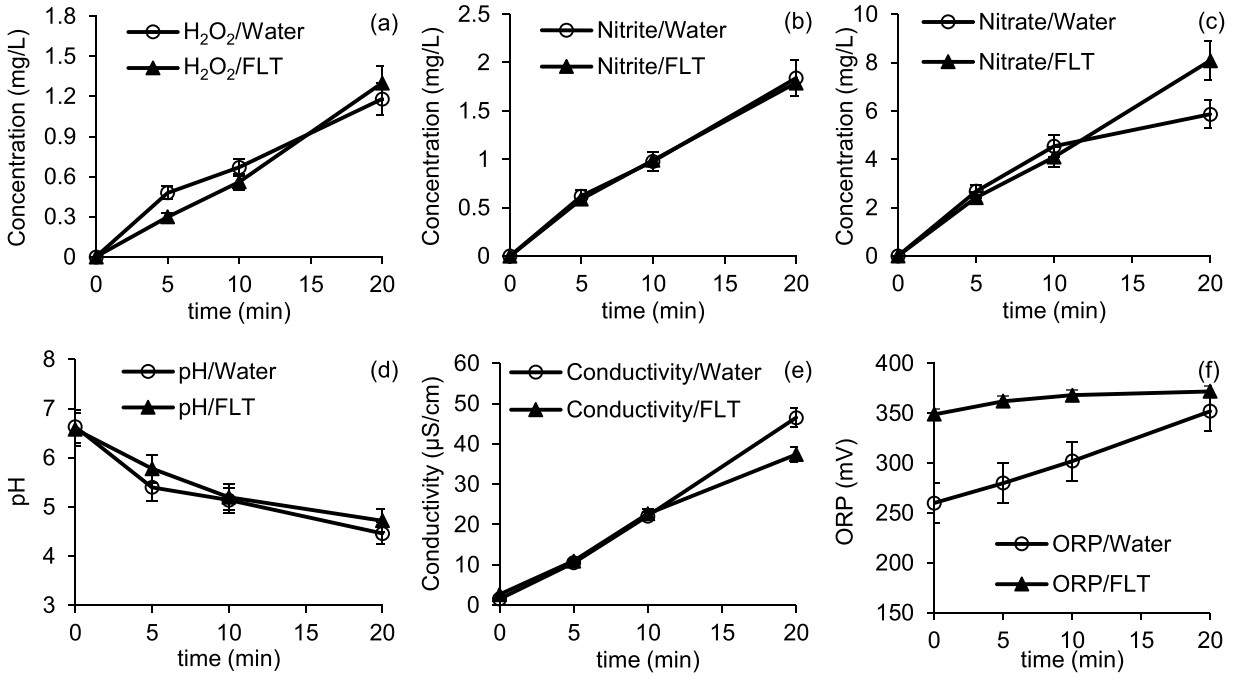

Fig. 5. Physicochemical properties of water versus time in the presence and absence of FLT. (a) H_2O_2, (b) NO_2^-, (c) NO_3^-, (d) pH, (e) conductivity, and (f) ORP (10 kV, 6 mm gap, 10 kHz, 1 μs, $C_0 = 0.2$ mg/L, $V = 100$ mL).

measured parameters changed during plasma exposure. The solution pH decreased from approximately 6.6 to 4.5, and conductivity, nitrite, nitrate, hydrogen peroxide, and oxidation-reduction potential (ORP) all steadily increased with longer discharge times, which is typical for air-plasma systems. Except for nitrite, the presence of FLT led to varying changes in these parameters compared to when

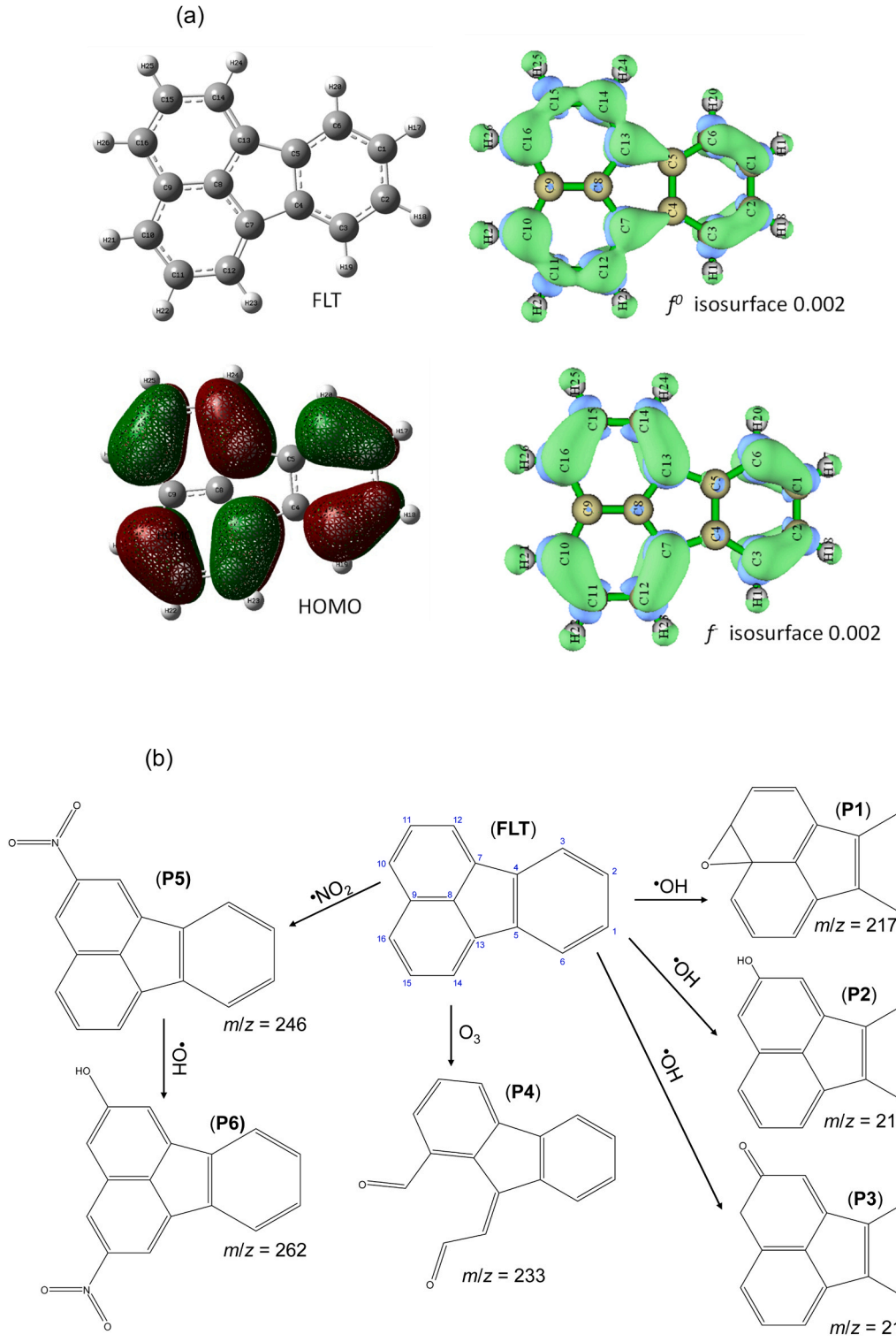

Fig. 6. (a) DFT calculation: optimised FLT molecule structure, HOMO orbitals, and Fukui functions; (b) Degradation pathway of FLT by air-NTP (*m/z* values are for [M-H]).

FLT was absent, particularly for ORP and hydrogen peroxide. ORP consistently increased in pure water exposed to plasma, indicating that oxidative species diffused into bulk water, increasing its tendency to form an oxidising medium. The ORP change in the absence of FLT was approximately 35 %, whereas in the presence of FLT, the change was only about 7 %. This lower change in ORP suggests that oxidative species are consumed by reactions with FLT.

Interestingly, the plot representing H_2O_2 concentrations reveals the consumption of hydrogen peroxide during the first 10 min of plasma exposure (the curve of H_2O_2/FLT is below the curve H_2O_2/water – Fig. 5), which could be indicative of the reactivity of these species toward the pollutant. With regard to nitrates, saturation is observed after 10 min of plasma treatment of water without FLT, but in the presence of FLT, saturation does not occur, at least within the time range used in this study. This can be attributed to the decomposition of peroxonitrite to $^{\bullet}OH$ and $NO_2^{\bullet}$ radicals, as described by the following reaction:

$$ONOOH_{(aq)} \rightarrow NO_{2(aq)}^{\bullet} + {}^{\bullet}OH_{(aq)} \quad (7)$$

The redox potential of the $ONOO^{\cdot}/NO_2^{\bullet}$ couple is closely aligned with that of the $^{\bullet}OH/H_2O$ couple (E° (Ox/Red),V/SHE 2.44 vs. E° (Ox/Red),V/SHE 2.85), making it a strong candidate for nitration reactions in the liquid phase (Brisset and Hnatiuc, 2012).

3.4. FLT degradation mechanism

The degradation products of FLT induced by NTP were determined using the Ultivo triple quadrupole mass spectrometer. A summary of the detected (DPs) and their corresponding CID fragments is provided in Table S2. Based on the identified compounds and the Fukui function indices, a proposed mechanism for FLT degradation by air-NTP is outlined (Figs. 6, 7).

Considering the products identified in Table S2, FLT degradation by air-NTP is suggested to occur through two distinct mechanisms, as illustrated in Fig. 6b: one involving reactive oxygen species ($^{\bullet}OH$ and O_3), and the other involving reactive nitrogen species ($^{\bullet}NO$ and $^{\bullet}NO_2$). It is anticipated that radical reactions will primarily occur at the atom with the highest Fukui function (f^0) value, while O_3 will attack the site of the highest occupied molecular orbital (HOMO) (von Sonntag and von Gunten, 2012; Lee et al., 2015). The structure of the FLT molecule suggests that reactive carbon sites are either at the edges, terminating in an attached hydrogen, or on the carbon atoms shared between neighbouring rings. Due to the molecule's symmetry, there are five distinct edge carbon sites and five shared carbon sites that can participate in these different reactions (Fig. 6a).

The probable site of radical attack on the FLT molecule was identified based on the highest Fukui function (f^0) value, indicating that C9 is the most likely site for radical attack. Thus, a possible mechanism involves $^{\bullet}OH$ addition to the shared reactive site C9, followed by oxygen reacting with the adduct via either HO_2 elimination or direct O_2 addition (Xing et al., 2020). In this mechanism, the hydrogen atom on the hydroxyl group is abstracted by O_2, which is followed by the O atom of the OH group reacting with a carbon atom at the ortho position of the aromatic ring, resulting in the formation of an aromatic ether (**P1**). Additionally, $^{\bullet}OH$ could attack C11 (or C15) leading to hydroxylation of FLT (**P2**), and further oxidation, involving electron transfer and subsequent disproportion,

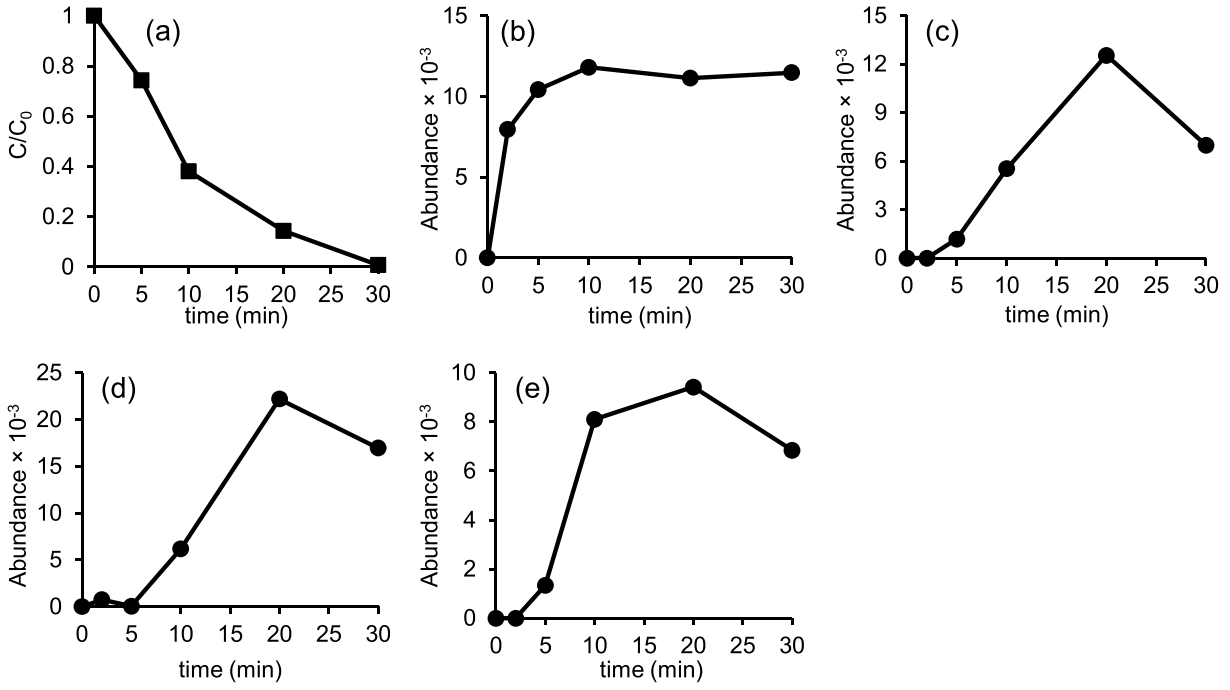

Fig. 7. Effect of reaction time on: (a) FLT concentration ratio, and abundance of products with *m/z* values of: (b) 217 P1 + P2 + P3, (c) 233 P4, (d) 246 P5, and (e) 262 P6.

could lead to the formation of an aromatic ketone (**P3**). Thus, radical attacks can take place preferentially at carbons either shared between neighbouring benzene rings or at the edges of the rings. A dynamic equilibrium exists between P2 and P3, two fundamentally equivalent structures, facilitating proton transfer to unsaturated ketones and allylic alcohols (Di Cosimo et al., 2005).

The HOMO-LUMO energy gap was used to assess the relative stability of products P1, P2 and P3. A larger gap between the highest occupied molecular orbital (HOMO) and the least occupied molecular orbital (LUMO) typically indicates lower chemical reactivity and higher kinetic stability. This is because it is energetically harder to excite an electron from the HOMO to the LUMO. Consequently, compounds with a larger HOMO-LUMO energy gap are generally more stable. The energy gaps for P1, P2, and P3 were 0.08947, 0.14448, and 0.13484 a.u., respectively (Fig. S1), suggesting that P2 is more stable than P3, and P1 is the least stable. These values of energy gaps were calculated using Gaussian from the HOMO and LUMO values of the optimised molecular structures of P1, P2, and P3.

An alternative attack mechanism involves an ozone-olefin reaction pathway. This pathway involves the formation of an ozonide and its breakdown, leading to the opening of the ring and the elimination of water to produce product (**P4**) (von Sonntag and von Gunten, 2012). According to the HOMO cloud (Fig. 6a), C10 (or C16) is likely the site of ozone attack, which is further supported by the Fukui function f^- map (Fig. 6a), where the green isosurface colour indicates regions of positive f^-, suggesting favourable reactive sites for electrophilic attack.

Products **P1-P3** all show *m/z* values of 217 [M-H]. As depicted in Fig. 7, the abundance signal for *m/z* 217 initially rises rapidly, reaching a peak within about 10 min, before plateauing. The slowdown in the production rate of *m/z* 217 may be due to competing reactions that lead to the formation of other products. In contrast, the kinetics for **P4** (*m/z* 233) display an initial lag of approximately 2 min before **P4** was detected, followed by a gradual increase in the abundance signal. This increase continues at a slower rate for about 20 min, after which the compound begins to degrade, as indicated by a decline in abundance between 20 and 30 min.

In addition to reactive oxygen species (ROS), reactive nitrogen species (RNS) reactions are also expected due to the use of air as the plasma gas. Nitric oxide ($NO^{\bullet}$) and nitrogen dioxide ($NO_2^{\bullet}$) radicals in the gas phase, along with liquid-phase peroxynitrite ions ($ONOO^-$), are typically the dominant species in RNS reactions (Lukes et al., 2014; Bruggeman et al., 2016; Bruno et al., 2020). Radical reactions initiated by $NO^{\bullet}$ and $NO_2^{\bullet}$ can lead to the addition of their respective groups to the FLT molecule through one-electron oxidation reaction. However, FLT-NO (i.e. *m/z* 230) was not detected in any of the samples, suggesting that NO radical attack is not a significant pathway. In contrast, FLT-NO_2 (**P5** *m/z* 246) was detected in significant abundance as shown in Fig. 7. The formation of P5 exhibited a lag of about 5 min before detection, after which its abundance increased, peaking before declining after 20 min.

A non-radical mechanism driven by peroxynitrous acid/peroxynitrite ($ONOOH \Leftrightarrow ONOO^- + H^+$, pka of 6.8 (Radi, 2013)), also contributes to FLT hydroxylation and nitration through the reactions of secondary $^{\bullet}OH$ and $NO_2^{\bullet}$. These species form at pH < 6.8 by the H^+-catalysed decomposition of peroxynitrite ($O{=}NOOH \Leftrightarrow {}^{\bullet}OH + NO_2^{\bullet}$) (Koppenol et al., 1992; Lukes et al., 2014). Both $^{\bullet}OH$ and $NO_2^{\bullet}$ were found to react with FLT, producing compound **P6**, which was detected after a 2-min lag and reached a maximum signal at 20 min, after which it began to degrade. Other possible intermediates were also detected, and their structures are listed in Table S2 (i.e. OI1, OI2, OI3). Further oxidation of the intermediates will lead to ring opening and eventual complete degradation to CO_2, H_2O, and nitrates. Nitrates result primarily from RNS attack rather than from the FLT structure itself.

Despite the effectiveness of NTP in degrading FLT demonstrated in this study, several limitations should be acknowledged. The primary limitation is that experiments were conducted under controlled laboratory conditions using synthetic FLT-contaminated water, and the NTP system's performance may differ in real environmental matrices where factors like co-contaminants, natural organic matter, and variations in pH or conductivity could impact plasma chemistry and treatment efficiency. Although degradation by-products were identified in this study, their full toxicological profiles and environmental persistence were not investigated, which presents a gap in assessing the complete safety and sustainability of the process. Moreover, the energy efficiency, while promising (up to 110 mg/kWh), still requires optimisation for scale-up applications. Thus, we recommend that future work should address these limitations using actual contaminated water matrices and conducting ecotoxicity assessments. It may be that hybrid systems that integrate NTP with other treatment technologies such as biological or adsorption-based post-treatments will be required. Investigating long-term reactor operation stability and the feasibility of continuous flow NTP systems for real-world deployment should also be examined. These efforts will be essential to advance NTP as a robust, scalable technology for PAH remediation in aquatic environments.

4. Conclusions

The experimental results presented in this article show that the degradation of FLT was rapid with a pseudo-first-order reaction rate constant proportional to the applied voltage. For most conditions studied, 80 % elimination of FLT was achieved in 5 min or less. As a result, the energy yield was high reaching a level of 110 mg/kWh and the degradation reached 100 % in less than 5 min. Best practical conditions ensuring both high degradation removals and plasma stability were 10 kV, 10 kHz, 1 μs, and 6 mm gap.

The stable species and physicochemical parameters measured in the liquid phase show varying changes over time, both in the presence and absence of FLT. For instance, the pH of the solution decreased from around 6.6–4.5; in contrast, the oxidation-reduction potential (ORP) consistently increased in pure water exposed to plasma, indicating that oxidative species diffused into bulk water, increasing its tendency to form an oxidising medium. The ORP change in the absence of FLT was approximately 35 %, whereas in the presence of FLT, the change was only about 7 %. This lower change of ORP in the presence of FLT suggests that oxidative species are consumed by FLT reactions. The change of H_2O_2 concentrations in the absence and presence of FLT revealed its contribution to FLT degradation, particularly, during the first 10 min of plasma exposure.

Analysis of FLT degradation products using LC-ESI-MS/MS identified nine compounds, primarily resulting from FLT hydroxylation and nitration. Fukui function indices for radical and electrophilic reactions were employed to elucidate a plausible mechanism for the

degradation of FLT. This approach, which models potential attack sites, could enable the design of controlled oxidation reactions and direct the production of specific species in the plasma phase by selecting appropriate plasma gases and powers.

Overall, the chemistry of FLT degradation by air-NTP is highly complex, involving a wide range of reactive species and competing reactions. This study highlights the potential of NTP for the effective degradation of PAHs. Additionally, the findings from this study suggest a promising strategy for optimising plasma reactors in the degradation of chemically stable and atypical molecules, such as PAHs, offering significant potential for improved applications in environmental and industrial settings. However, challenges such as scalability using real contaminated waters, energy consumption, and potential secondary by-products need to be addressed for widespread implementation. Continued research and technological advancements could help overcome these limitations and improve the practical applicability of NTP for large-scale water treatment.

CRediT authorship contribution statement

Djakaou Iya-Sou: Writing – review & editing, Writing – original draft, Methodology, Formal analysis, Data curation, Conceptualization. **Chedly Tizaoui:** Writing – review & editing, Supervision, Resources, Project administration, Methodology, Investigation, Funding acquisition, Formal analysis, Conceptualization. **Nofel Merbahi:** Writing – review & editing, Visualization, Supervision, Project administration, Methodology, Funding acquisition, Data curation, Conceptualization. **Jalloul Bouajila:** Writing – review & editing, Visualization, Supervision, Project administration, Methodology, Formal analysis, Data curation, Conceptualization.

Declaration of Competing Interest

The authors declare that they have no known competing financial interests or personal relationships that could have appeared to influence the work reported in this paper.

Acknowledgement

CT and NM acknowledge the support received from the Ministry of Higher Education, Research and Innovation, France, under the Invited Professors program.

Appendix A. Supporting information

Supplementary data associated with this article can be found in the online version at doi:10.1016/j.eti.2025.104390.

Data availability

Data will be made available on request.

References

Abbas, Y., Lu, W., Dai, H., Fu, X., Ye, R., Wang, H., 2020. Remediation of polycyclic aromatic hydrocarbons (PAHs) contaminated soil with double dielectric barrier discharge plasma technology: influencing parameters. Chem. Eng. J. 394, 124858.

Abdelaziz, A.A., Ishijima, T., Tizaoui, C., 2018. Development and characterization of a wire-plate air bubbling plasma for wastewater treatment using nanosecond pulsed high voltage. J. Appl. Phys. 124, 12.

Agency for Toxic Substances and Disease Registry (US), 1995. Toxicological profile for polycyclic aromatic hydrocarbons. Atlanta (GA). 2, Health effects. ⟨https://www.ncbi.nlm.nih.gov/books/NBK598180/⟩.

Bai, H., Zhou, J., Zhang, H., Tang, G., 2017. Enhanced adsorbability and photocatalytic activity of TiO2-graphene composite for polycyclic aromatic hydrocarbons removal in aqueous phase. Colloids Surf. B Biointerfaces 150, 68–77.

Bilea, F., Bradu, C., Medvedovici, A.V., Hong, D., Magureanu, M., 2024. Pulsed corona discharge: an advanced treatment method for antibiotic-contaminated water. J. Phys. D Appl. Phys. 57, 435205.

Boström, C.E., Gerde, P., Hanberg, A., Jernström, B., Johansson, C., Kyrklund, T., Rannug, A., Törnqvist, M., Victorin, K., Westerholm, R., 2002. Cancer risk assessment, indicators, and guidelines for polycyclic aromatic hydrocarbons in the ambient air. Environ. Health Perspect. 110 (3), 451–488.

Brisset, J.-L., Hnatiuc, E., 2012. Peroxynitrite: A Re-examination of the Chemical Properties of Non-thermal Discharges Burning in Air Over Aqueous Solutions. Plasma Chem. Plasma Process. 32, 655–674.

Bruggeman, P.J., Kushner, M.J., Locke, B.R., Gardeniers, J.G.E., Graham, W.G., Graves, D.B., Hofman-Caris, R.C.H.M., Maric, D., Reid, J.P., Ceriani, E., Fernandez Rivas, D., Foster, J.E., Garrick, S.C., Gorbanev, Y., Hamaguchi, S., Iza, F., Jablonowski, H., Klimova, E., Kolb, J., Krcma, F., Lukes, P., Machala, Z., Marinov, I., Mariotti, D., Mededovic Thagard, S., Minakata, D., Neyts, E.C., Pawlat, J., Petrovic, Z.L., Pflieger, R., Reuter, S., Schram, D.C., Schröter, S., Shiraiwa, M., Tarabová, B., Tsai, P.A., Verlet, J.R.R., von Woedtke, T., Wilson, K.R., Yasui, K., Zvereva, G., 2016. Plasma–liquid interactions: a review and roadmap. Plasma Sources Sci. Technol. 25, 053002.

Bruno, G., Wenske, S., Lackmann, J.-W., Lalk, M., von Woedtke, T., Wende, K., 2020. On the liquid chemistry of the reactive nitrogen species peroxynitrite and nitrogen dioxide generated by physical plasmas. Biomolecules 10, 1687.

Di Cosimo, J.I., Acosta, A., Apesteguía, C.R., 2005. Allylic alcohol synthesis by gas-phase hydrogen transfer reduction of unsaturated ketones. J. Mol. Catal. A Chem. 234, 111–120.

Dickenson, A., Walsh, J.L., Hasan, M.I., 2021. Electromechanical coupling mechanisms at a plasma–liquid interface. J. Appl. Phys. 129.

Djakaou, I.-S., Ghezzar, R.M., Zekri, M.E.-M., Abdelmalek, F., Cavadias, S., Ognier, S., 2015. Removal of model pollutants in aqueous solution by gliding arc discharge. Part II: modeling and simulation study. Plasma Chem. Plasma Process. 35, 143–157.

EA&DEFRA, 2025. Surface water pollution risk assessment for your environmental permit.⟨https://www.gov.uk/guidance/surface-water-pollution-risk-assessment-for-your-environmental-permit⟩.
Environment Agency, 2019. Polycyclic aromatic hydrocarbons (PAHs): sources, pathways and environmental data. ⟨https://consult.environment-agency.gov.uk/++preview++/environment-and-business/challenges-and-choices/user_uploads/polycyclic-aromatic-hydrocarbons-rbmp-2021.pdf⟩.
Environmental Protection Agency, ⟨https://www.govinfo.gov/content/pkg/CFR-2014-title40-vol29/pdf/CFR-2014-title40-vol29-part423-appA.pdf⟩.
EPA, 1980. Ambient water quality criteria for fluoranthene. ⟨https://www.epa.gov/sites/default/files/2019-03/documents/ambient-wqc-fluoranthene-1980.pdf⟩.
Farooq, S., Cai, R., McGettrick, J., Pean, E., Davies, M., Al Harrasi, A.S., Palmer, R., Tizaoui, C., 2023. Visible-light induced photocatalytic degradation of estrone (E1) with hexagonal copper selenide nanoflakes in water. Process Saf. Environ. Prot. 172, 1–15.
Fei, C., 2012. Comparison of computational methods for atomic charges. Acta Phys. Chim. Sin.
Furusato, T., Sasaki, M., Matsuda, Y., Yamashita, T., 2022. Underwater shock wave induced by pulsed discharge on water. J. Phys. D Appl. Phys. 55, 115203.
Galindo, M.V., Hantao, L.W., Sampaio, N.M.F.M., Pessoto, M.A., Oliveira, W.D.S., Godoy, H.T., 2025. Analysis of polycyclic aromatic hydrocarbons in Brazilian human milk: a simple and effective approach. Food Control 167.
Gao, L., Sun, L., Wan, S., Yu, Z., Li, M., 2013. Degradation kinetics and mechanism of emerging contaminants in water by dielectric barrier discharge non-thermal plasma: the case of 17β-Estradiol. Chem. Eng. J. 228, 790–798.
Hamdan, A., Liu, J.-L., Cha, M.S., 2018. Microwave plasma jet in water: characterization and feasibility to wastewater treatment. Plasma Chem. Plasma Process. 38, 1003–1020.
Hosea, L., Salvidge, R., 2024. Almost 500 chemicals found in England's rivers and groundwater. The Guardian. ⟨https://www.theguardian.com/environment/article/2024/aug/06/almost-500-chemicals-found-in-englands-rivers-and-groundwater⟩.
Iya-Sou, D., Merbahi, N., Bouajila, J., Yousfi, M., 2024. Air pulsed-corona discharges for degradation of emerging pharmaceutical pollutants in water and toxicity by-products control. J. Water Process Eng. 67, 106127.
Iya-Sou, D., Merbahi, N., Bouajila, J., Yousfi, M., 2025. Study and scaling-up of multi-tip pulsed-corona air discharges for degradation of paracetamol. J. Phys. D Appl. Phys. 58, 025202.
Ji, Z., Zhang, N., Huang, C., Duan, X., Ren, D., Huo, Z., 2024. The degradation of polycyclic aromatic hydrocarbons (PAHs) by ozone-based advanced oxidation processes: a review. Ozone Science Engineering 46, 26–42.
Khourshidi, A., Ajam, F., Rabieian, M., Taghavijeloudar, M., 2024. Efficient degradation of p-nitrophenol from water by enhancing dielectric barrier discharge (DBD) plasma through ozone circulation: optimization, kinetics and mechanism. Chemosphere 362, 142749.
Kim, H.-J., Won, C.-H., Kim, H.-W., 2020. Optimized pretreatment of non-thermal plasma for advanced sewage oxidation. Int. J. Environ. Res. Public Health 17, 7694.
Kong, X.Z., Zhang, H., Li, X.D., Xu, R.Y., Mubeen, I., Li, L., Yan, J.H., 2019. Destruction of toluene, naphthalene and phenanthrene as model tar compounds in a modified rotating gliding arc discharge reactor. Catalysts 9.
Kooshki, S., Pareek, P., Janda, M., Machala, Z., 2024. Selective reactive oxygen and nitrogen species production in plasma-activated water via dielectric barrier discharge reactor: an innovative method for tuning and its impact on dye degradation. J. Water Process Eng. 63, 105477.
Koppenol, W.H., Moreno, J.J., Pryor, W.A., Ischiropoulos, H., Beckman, J.S., 1992. Peroxynitrite, a cloaked oxidant formed by nitric oxide and superoxide. Chem. Res. Toxicol. 5, 834–842.
Lee, M., Zimmermann-Steffens, S.G., Arey, J.S., Fenner, K., von Gunten, U., 2015. Development of prediction models for the reactivity of organic compounds with ozone in aqueous solution by quantum chemical calculations: the role of delocalized and localized molecular orbitals. Environ. Sci. Technol. 49, 9925–9935.
Locke, B.R., Sato, M., Sunka, P., Hoffmann, M.R., Chang, J.S., 2006. Electrohydraulic discharge and nonthermal plasma for water treatment. Ind. Eng. Chem. Res. 45, 882–905.
Locke, B.R., Thagard, S.M., Lukes, P., 2025. Recent insights into interfacial transport and chemical reactions of plasma-generated species in liquid. Plasma Process. Polym. 22, 2400207.
Lu, T., Chen, F., 2012. Multiwfn: a multifunctional wavefunction analyzer. J. Comput. Chem. 33, 580–592.
Lu, T., Chen, Q., 2020. mwfn: A Strict, Concise and Extensible Format for Electronic Wavefunction Storage and Exchange. ChemRxiv.
Lukes, P., Dolezalova, E., Sisrova, I., Clupek, M., 2014. Aqueous-phase chemistry and bactericidal effects from an air discharge plasma in contact with water: evidence for the formation of peroxynitrite through a pseudo-second-order post-discharge reaction of H2O2 and HNO2. Plasma Sources Sci. Technol. 23, 015019.
Machala, Z., Tarabová, B., Sersenová, D., Janda, M., Hensel, K., 2019. Chemical and antibacterial effects of plasma activated water: correlation with gaseous and aqueous reactive oxygen and nitrogen species, plasma sources and air flow conditions. J. Phys. D Appl. Phys. 52, 034002.
Montgomery, J., 2007. Groundwater Chemicals Desk Reference, forth ed. CRC Press. ⟨https://www.perlego.com/book/1710517/groundwater-chemicals-desk-reference-pdf⟩.
Murugesan, P., V, E.M., Moses, J.A., Anandharamakrishnan, C., 2020. Water decontamination using non-thermal plasma: concepts, applications, and prospects. J. Environ. Chem. Eng. 8, 104377.
Nippatlapalli, N., Locke, B.R., 2022. Integrating nonthermal plasma with conventional technology for water pollution treatment. Int. J. Plasma Environ. Sci. Technol. 16, e02006.
Popov, P., Getoff, N., 2005. Radiation-induced degradation of aqueous fluoranthene. Radiat. Phys. Chem. 72, 19–24.
PubChem, 2023. Fluoranthene. ⟨https://pubchem.ncbi.nlm.nih.gov/compound/Fluoranthene⟩.
Radi, R., 2013. Peroxynitrite, a Stealthy Biological Oxidant. J. Biol. Chem. 288, 26464–26472.
Saleem, M., Tomei, G., Beria, M., Marotta, E., Paradisi, C., 2022. Highly efficient degradation of PFAS and other surfactants in water with atmospheric RAdial plasma (RAP) discharge. Chemosphere 307, 135800.
Shao, T., Wang, R., Zhang, C., Yan, P., 2018. Atmospheric-pressure pulsed discharges and plasmas: mechanism, characteristics and applications. High. Volt. 3, 14–20.
Shen, J., Zhang, H., Xu, Z., Zhang, Z., Cheng, C., Ni, G., Lan, Y., Meng, Y., Xia, W., Chu, P.K., 2019. Preferential production of reactive species and bactericidal efficacy of gas-liquid plasma discharge. Chem. Eng. J. 362, 402–412.
von Sonntag, C., von Gunten, U., 2012. Chemistry of Ozone in Water and Wastewater Treatment: From Basic Principles to Applications. IWA Publishing.
Styszko, K., Pamuła, J., Sochacka-Tatara, E., Pac, A., Kasprzyk-Hordern, B., 2025. Estimation of public exposure to PAH and environmental risks via wastewater-based epidemiology. Ecotoxicol. Environ. Saf. 292, 117920.
Sun, K., Song, Y., Liu, Z., Jing, M., Wan, J., Tang, J., Liu, R., 2020. Toxicity assessment of Fluoranthene, Benz(a)anthracene and its mixed pollution in soil: Studies at the molecular and animal levels. Ecotoxicol. Environ. Saf. 202, 110864.
Tachibana, K., Nakamura, T., 2019. Comparative study of discharge schemes for production rates and ratios of reactive oxygen and nitrogen species in plasma activated water. J. Phys. D Appl. Phys. 52, 385202.
Tovar-Salvador, M.L., Rios-Quintero, R., Pintado-Herrera, M.G., Palacios-Miñambres, M., Lara-Martín, P.A., 2025. Occurrence of priority and emerging organic contaminants in cold-water corals and their habitat: a case study in La Herradura Bay (Spain). Mar. Environ. Res. 204.
Tufail, A., Price, W.E., Hai, F.I., 2020. A critical review on advanced oxidation processes for the removal of trace organic contaminants: a voyage from individual to integrated processes. Chemosphere 260, 127460.
Wang, Y., Song, J., Zhu, R., Peng, M., Long, J., Bao, T., 2025. Degradation of pharmaceutical contaminants in wastewater by non-thermal plasma technology: a comprehensive Review. J. Environ. Chem. Eng. 13, 116150.
Wu, L., Xie, Q., Lv, Y., Zhang, Z., Wu, Z., Liang, X., Lu, M., Nie, Y., 2019. Degradation of methylene blue by dielectric barrier discharge plasma coupled with activated carbon supported on polyurethane foam. RSC Adv. 9, 25967–25975.
Wu, J., Xu, G., Xia, F., Liu, X., Zheng, L., 2023. Comparison of the sensitivity between indigenous and exotic aquatic species for fluoranthene and derivation of water quality criteria (WQC). Environ. Sci. Pollut. Res. 30, 7617–7624.
Xing, L., Meng, Q., Zhang, L., 2020. A thorough theoretical mechanistic study of OH-initiated oxidative degradation mechanism for large polycyclic aromatic hydrocarbons. Comput. Theor. Chem. 1175, 112730.

Xiong, Y., Zhang, Q., Wandell, R., Bresch, S., Wang, H., Locke, B.R., Tang, Y., 2019. Synergistic 1,4-dioxane removal by non-thermal plasma followed by biodegradation. Chem. Eng. J. 361, 519–527.
Zhan, J., Liu, Y., Cheng, W., Zhang, A., Li, R., Li, X., Ognier, S., Cai, S., Yang, C., Liu, J., 2018. Remediation of soil contaminated by fluorene using needle-plate pulsed corona discharge plasma. Chem. Eng. J. 334, 2124–2133.
Zhang, J., Feng, Y., Hu, T., Xu, X., Zhao, D., Zhao, J., Wang, X., Li, L., Wang, S., Song, C., Zhao, S., 2024. Antibiotics and polycyclic aromatic hydrocarbons in marine food webs of the Yellow River Estuary: occurrence, trophic transfer, and human health risks. Sci. Total Environ. 943.
Zhang, J., Huang, H., Wang, R., Sun, R., 2019. Historical pollution and source contributions of PAHs in sediment cores from the middle reach of Huai River, China. Bull. Environ. Contam. Toxicol. 102, 531–537.
Ziyaei, K., Mokhtari, M., Hashemi, M., Rezaei, K., Abdi, F., 2024. Association between exposure to water sources contaminated with polycyclic aromatic hydrocarbons and cancer risk: a systematic review. Sci. Total Environ. 924, 171261.